Extension of Analytic Results for a PT-Symmetric Structure

H. F. Jones[†] and M. Kulishov[‡]

[†]*Physics Department, Imperial College, London SW7 2BZ, UK*
[‡]*HTA Photomask, 1605 Remuda Lane, San Jose, CA 95112, USA*

The PT-symmetric optical grating with index profile $e^{2i\beta z}$ has been shown to have the interesting property of being essentially invisible for light incident from one side, while possessing greatly enhanced reflection at a particular wavelength for light incident from the other side. We extend a previous analysis of this grating to obtain an analytic solution for the case when the grating is embedded on a substrate, with different refractive indices on either side. We also generalize the previous case of normal incidence to incidence at an arbitrary angle. In that case the enhanced reflection occurs at a particular angle of incidence for a given wavelength. Finally we discuss how the grating may be used to give lasing.

PACS numbers: 42.25.Bs, 02.30.Gp, 11.30.Er, 42.82.Et

I. INTRODUCTION

The ideas of PT symmetry, originally introduced in the context of quantum mechanics[1]-[6], have recently led to rapid developments in the apparently unconnected field of classical optics[7]-[16]. The connection arises from the fact that when one makes the paraxial approximation for the equation of propagation of an electromagnetic wave the resulting equation is formally identical to the Schrödinger equation, but with different interpretations for the symbols appearing therein. In particular, the role of time in the Schrödinger equation is taken by the longitudinal coordinate z, while that of the quantum-mechanical potential is taken by variations of the refractive index of the medium in the transverse x direction. PT-symmetry deals with potentials that are not Hermitian, which translates in optics to complex refractive indices. It is extremely common for the refractive index to have a positive imaginary part, corresponding to loss, but a negative imaginary part can also be implemented by optical pumping, leading to gain. PT-symmetry requires that loss and gain be balanced in a particular way, namely that $n^*(-x) = n(x)$, or equivalently that $\mathrm{Re}(n)$ be an even function and $\mathrm{Im}(n)$ an odd function of x. When the PT symmetry is unbroken this leads to real propagation constants, i.e. no exponential growth or decay even in the presence of gain and loss.

Although this connection was first made explicit in Ref. [7], the exotic properties of materials with combined gain and loss were previously explored in Refs. [17] and [18]. In those papers the index modulation was in the z direction rather than the transverse x direction. In that case, if we consider H-mode polarization, in which the electric field is transverse, the equation of propagation for a given component of the electric field is just the scalar Helmholtz equation

$$\left[d^2/dz^2 + k^2(n(z)/n_0)^2\right] E(z) = 0, \tag{1}$$

which can be compared to the time-independent Schrödinger equation.

Of particular interest is the PT-symmetric profile $n(z) \propto \cos(\beta z) + i\lambda \sin(\beta z)$, discussed by Lin et al.[19]. The symmetry is preserved in the spectrum for $\lambda < 1$, in which case a similarity transformation can be made to the Hermitian Mathieu potential[20, 21], but broken for $\lambda \geq 1$. The non-linear version of this potential, with Kerr nonlinearity, has also been considered, and analytic solitonic solutions obtained[22].

Precisely at the symmetry-breaking point $\lambda = 1$, the variation in $n(z)$ becomes a pure complex exponential proportional to $e^{i\beta z}$. This potential, which had been previously considered by Kulishov et al.[23], exhibits to a good approximation the intriguing phenomenon of "unidirectional invisibility" for normal incidence, with perfect transmission from left or right and zero reflection from the left. On the other hand, for right incidence, the concomitant property is a greatly enhanced reflectivity, sharply peaked at $k = \beta$. An experimental set-up demonstrating invisibility, albeit for a "passive" situation, whereby only the lossy part of the potential is used, was subsequently given by Feng et al. [24].

In Refs. [25] and [26] an analytic solution was found for the scattering coefficients in terms of Bessel functions, showing the limitations of the coupled-mode approximation used in Refs. [19, 23]. It was shown that for the parameters used in that paper there were small deviations from invisibility, and that the property broke down completely for much longer lengths of the grating, when the straightforward coupled-wave approximation becomes unreliable[25, 27].

These papers were concerned with the one-dimensional situation described by Eq. (1), that is, for normal incidence on the lattice (as shown in Figs. 1 and 2 below). However, it is of interest to generalize this situation in two ways. First one can consider incidence at an angle, and secondly the situation when the grating is superimposed on a material of different refractive index than those on either side. This problem has recently been addressed in Ref. [28], but in the context of the Bragg approximation method, with analytic expressions obtained for the first three Bragg orders. In the present paper we demonstrate that the method of Ref. [26] can be extended to deal with both these generalizations, yielding analytic expressions for the reflection and transmission coefficients in terms of modified Bessel functions. Our results can be used to check the approximations used in Ref. [28], but are applicable for a much wider range of parameters.

In the following Sec. II we briefly review the methodology and results of Ref. [26]. Then in Sec. III we generalize the analysis to include non-normal incidence and different refractive indices on either side of the grating. These results are then used in Sec. IV to produce graphs of transmission and reflection coefficients, as a function of angle, in a variety of different configurations. In Sec. V we revert to the one-dimensional situation and consider placing a mirror at one end of the grating, showing that, because of the enhanced reflectivity of the grating, the cavity can lase when its strength exceeds a certain critical value. Finally, in Sec. VI, we give our conclusions.

II. ANALYTIC SOLUTION FOR RESTRICTED CASE

The set-up dealt with in Refs. [19], [25], [26] is shown in Fig. 1 (for left incidence). We recall here the results of Ref. [26] for completeness and comparison with the results in the more general case.

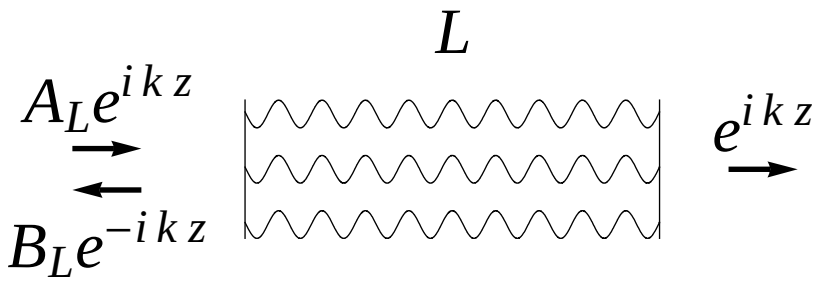

FIG. 1: Set-up for propagation from the left

The situation is essentially one-dimensional, and Eq. (1) reduces to

$$\frac{d^2E}{dz^2} + k^2(1 + 2v(z))E = 0, \tag{2}$$

where $v(z)$ has the special form $v(z) = \frac{1}{2}\alpha^2 e^{2i\beta z}$.

Changing variables to $y = (k\alpha/\beta)e^{i\beta z}$, the equation becomes

$$y^2\frac{d^2E}{dy^2} + y\frac{dE}{dy} - (y^2 + k^2/\beta^2)E = 0, \tag{3}$$

which is the modified Bessel equation, with solution $E = CI_\nu(y) + DK_\nu(y)$, where $\nu = k/\beta$. In the language of quantum mechanics ($\psi \equiv E$),

$$\psi(z) = CI_\nu(y) + DK_\nu(y) \tag{4}$$

This has to be matched on to $\psi = A_\pm e^{ikz} + B_\pm e^{-ikz}$ at $z = \pm L/2$.

A. Left Incidence

By requiring that $\psi(L/2) = e^{ikL/2}$ and $\psi'(L/2) = ike^{ikL/2}$ we find that

$$\begin{aligned} C &= y_+ K_{\nu+1}(y_+)e^{ikL/2} \\ D &= y_+ I_{\nu+1}(y_+)e^{ikL/2}, \end{aligned}$$

where $y_\pm \equiv \nu\alpha\ e^{\pm i\beta L/2}$, so that

$$\psi(z) = y_+ \left[K_{\nu+1}(y_+)I_\nu(y) + I_{\nu+1}(y_+)K_\nu(y)\right] e^{ikL/2} \tag{5}$$

Both initial conditions are satisfied by virtue of the various recursion relations among the modified Bessel functions and the Wronskian identity[29]

$$K_{\nu+1}(y)I_\nu(y) + I_{\nu+1}(y)K_\nu(y) = 1/y\ . \tag{6}$$

At $z = -L/2$ we have to match ψ with $A_L e^{-ikL/2} + B_L e^{ikL/2}$. The general formulas are

$$A_L e^{ikz} = \frac{1}{2}[\psi(z) - (i/k)\psi'(z)]$$

$$B_L e^{-ikz} \;=\; \frac{1}{2}[\psi(z) + (i/k)\psi'(z)]$$

which give, after some algebra,

$$\begin{aligned} A_L \;&=\; (\frac{1}{2}\alpha^2\nu)e^{ikL}[K_{\nu+1}(y_+)I_{\nu-1}(y_-) - I_{\nu+1}(y_+)K_{\nu-1}(y_-)] \\ B_L \;&=\; (\frac{1}{2}\alpha^2\nu)e^{-ikL}[-K_{\nu+1}(y_+)I_{\nu+1}(y_-) + I_{\nu+1}(y_+)K_{\nu+1}(y_-)] \end{aligned} \tag{7}$$

B. Right Incidence

The set-up is shown in Fig. 2, with the transmitted amplitude again normalized to 1.

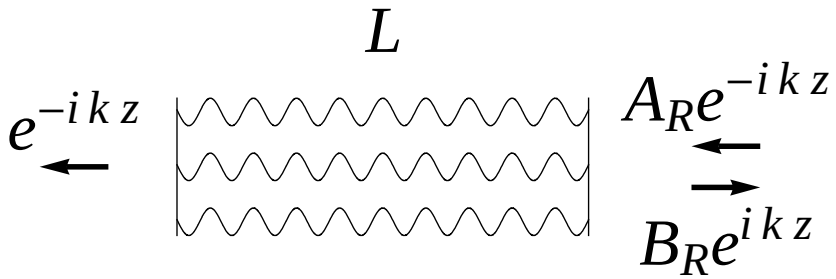

FIG. 2: Set-up for propagation from the right

The initial conditions are now $\psi(-L/2) = e^{ikL/2}$ and $\psi'(-L/2) = -ike^{ikL/2}$, which give

$$\begin{aligned} C \;&=\; y_- K_{\nu-1}(y_-)e^{ikL/2} \\ D \;&=\; y_- I_{\nu-1}(y_-)e^{ikL/2}, \end{aligned}$$

so that

$$\psi(z) = y_- \left[K_{\nu-1}(y_-)I_\nu(y) + I_{\nu-1}(y_-)K_\nu(y)\right] e^{ikL/2} \tag{8}$$

Again, the initial conditions are satisfied by virtue of Eq. (6).

At $z = L/2$ we have to match ψ with $A_R e^{-ikL/2} + B_R e^{ikL/2}$. The general formulas are

$$\begin{aligned} A_R e^{-ikz} \;&=\; \frac{1}{2}[\psi(z) + (i/k)\psi'(z)] \\ B_R e^{ikz} \;&=\; \frac{1}{2}[\psi(z) - (i/k)\psi'(z)] \end{aligned}$$

giving

$$\begin{aligned} A_R \;&=\; (\frac{1}{2}\alpha^2\nu)e^{ikL}[\;\; I_{\nu-1}(y_-)K_{\nu+1}(y_+) - K_{\nu-1}(y_-)I_{\nu+1}(y_+)] \\ B_R \;&=\; (\frac{1}{2}\alpha^2\nu)e^{-ikL}[-I_{\nu-1}(y_-)K_{\nu-1}(y_+) + K_{\nu-1}(y_-)I_{\nu-1}(y_+)] \end{aligned} \tag{9}$$

Note that the reflection amplitude B_R can be obtained from B_L by the transformations $y_+ \leftrightarrow y_-$ and $\nu \leftrightarrow -\nu$, which is a consequence of PT symmetry. Under those same transformations the transmission amplitude $A_L \equiv A_R$ is invariant. The equality of A_L and A_R is a general result, obtained most easily by evaluating the Wronskian of the two solutions $\psi_L(z)$ and $\psi_R(z)$ for $z < -L/2$ and $z > L/2$.

It is important to note that in the evaluation of Eqs. (7) and (9) the argument y of the Bessel functions encircles the origin and crosses the cut on the negative real axis many times as z goes from $-L/2$ to $L/2$. Thus it is important to know how to continue onto subsequent sheets. The relevant formulas (incorrectly quoted in Ref. [26]) are

$$\begin{aligned} I_\nu(ye^{im\pi}) &= e^{im\pi\nu} I_\nu(y) \\ K_\nu(ye^{im\pi}) &= e^{-im\pi\nu} K_\nu(y) - i\pi \frac{\sin(m\pi\nu)}{\sin(\pi\nu)} I_\nu(y), \end{aligned} \tag{10}$$

where m is an integer. Once these are implemented the resulting functions are smooth functions of z, with no discontinuities.

It is interesting to see how these exact results go over to the approximate results of the coupled-wave approximation, namely $T = 1$, $R_L = 0$ and $R_R = \left(\frac{1}{2}k\alpha^2 \sin(L\delta)/\delta\right)^2$. For a grating containing an even number of periods, $L = 2m\Lambda \equiv 2m\pi/\beta$, we use the preceding connection formulas to write $I_\nu(y_\pm)$ and $K_\nu(y_\pm)$ in terms of $I_\nu(y_0)$ and $K_\nu(y_0)$, where $y_0 = \nu\alpha$. Then the result for A_L is

$$\begin{aligned} A_L = \frac{1}{2}\alpha^2 \nu e^{ikL} \Big\{ & e^{-2im\pi\nu} K_{\nu+1}(y_0) I_{\nu-1}(y_0) - e^{2im\pi\nu} K_{\nu-1}(y_0) I_{\nu+1}(y_0) \\ & + i\pi \frac{\sin(2m\pi\nu)}{\sin(\pi\nu)} I_{\nu+1}(y_0) I_{\nu-1}(y_0) \Big\} \end{aligned} \tag{11}$$

The coupled-wave approximation amounts to weak coupling, i.e. taking $\alpha \ll 1$ and small detuning, i.e. $\delta \ll 1$, which corresponds to $\nu \sim 1$. In that case the functions $I_\nu(y_0)$ and $K_\nu(y_0)$ can be approximated as

$$I_\nu(y_0) \sim y_0^\nu \quad \text{and} \quad K_\nu(y_0) \sim y_0^{-\nu} \tag{12}$$

The leading term in the expression for A_L is then the first one, which simply gives $A_L \sim e^{ikL}$. The second and third terms are of order α^4.

A similar analysis for B_L gives

$$B_L = \frac{1}{2} i\alpha^2 \nu e^{-ikL} I_{\nu+1}(y_0) \left\{ 2\sin(2m\pi\nu) K_{\nu+1}(y_0) + i\pi \frac{\sin[2m\pi(\nu+1)]}{\sin(\pi\nu)} I_{\nu+1}(y_0) \right\}, \tag{13}$$

which vanishes in the above approximation.

Finally B_R becomes

$$B_R = \frac{1}{2} i\alpha^2 \nu e^{-ikL} I_{\nu-1}(y_0) \left\{ 2\sin(2m\pi\nu) K_{\nu-1}(y_0) + i\pi \frac{\sin[2m\pi(\nu-1)]}{\sin(\pi\nu)} I_{\nu-1}(y_0) \right\}. \tag{14}$$

The dominant contribution comes from the last term, yielding

$$B_R \sim \pm\frac{1}{2}i\alpha^2 e^{-ikL}\frac{\sin(2m\pi\nu)}{\sin(\pi\nu)} \sim \pm\frac{1}{2}ik\alpha^2 e^{-ikL}\frac{\sin(L\delta)}{\delta}. \tag{15}$$

near $\delta = 0$, in agreement with the coupled-wave result, with $R_R = |B_R/A|^2$. It is interesting to note that the characteristic sinc^2 shape of R_R arises precisely from the additional term proportional to $I_\nu(y)$ in the continuation formula for $K_\nu(ye^{im\pi})$.

III. ANALYTIC SOLUTION IN GENERAL CASE

In this section we generalize the previous results in two ways, by considering non-normal incidence allowing for different background refractive indices on either side of the grating.

A. Left Incidence

The set-up for left incidence is shown in Fig. 3.

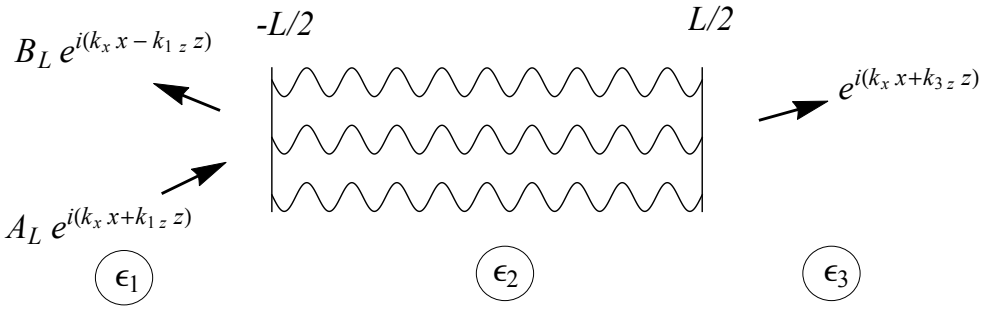

FIG. 3: Generalized set-up for propagation from the left

For incidence at an angle, there is an overall component of the wave, in, say, the x-direction, of the form $e^{ik_x x}$. So in Eq. (1) we can write E as $E(x,z) = e^{ik_x x}\psi(z)$, and the equation for $\psi(z)$ becomes

$$\frac{d^2\psi}{dz^2} + \left[k_2^2(1+\alpha^2 e^{2i\beta z}) - k_x^2\right]\psi = 0. \tag{16}$$

Here $k_2 = \sqrt{\varepsilon_2}k_0$, where $k_0 = 2\pi/\lambda$ is the free-space wave-vector. The appropriate definition of y is now $y = (k_2\alpha/\beta)e^{i\beta z}$, which again results in the modified Bessel equation

$$y^2\frac{d^2\psi}{dy^2} + y\frac{d\psi}{dy} - (y^2+\nu^2)\psi = 0, \tag{17}$$

with the difference that ν is now defined by

$$\nu^2 = \frac{k_2^2 - k_x^2}{\beta^2} \tag{18}$$

or in other words $\nu = k_{2z}/\beta = (k_2 \cos\theta)/\beta$, where θ is the internal angle of refraction. Thus y can be written as

$$y = \left(\frac{\nu\alpha}{\cos\theta}\right) e^{i\beta z}. \tag{19}$$

When considering non-normal incidence the boundary conditions depend on the polarization state of the input radiation. In this paper we will restrict ourselves to the simplest case of H-mode polarization, in which the $\boldsymbol{E}$-field is in the y-direction, and so parallel to the two interfaces at $z = \pm L/2$. In general the boundary conditions require that the tangential electric and magnetic fields be continuous across a boundary. In this case H_x is proportional to ψ', so the conditions are that ψ and ψ' be continuous, as before. The difference is that, for $\varepsilon_2 \neq \varepsilon_1$ and/or $\varepsilon_2 \neq \varepsilon_3$ the longitudinal wave-vectors in the three regions are unequal. Thus, given that $k_1 \sin\theta' = k_2 \sin\theta$, it is straightforward to show that $k_{1z} = \gamma_1\nu\beta$ and $k_{3z} = \gamma_3\nu\beta$, where $\gamma_r = \left(\varepsilon_r/\varepsilon_2 - \sin^2\theta\right)^{\frac{1}{2}} / \cos\theta$. In the previous case of equal background permittivities these reduced to $\gamma_1 = \gamma_2 = 1$.

Applying the boundary conditions of continuity for both ψ and ψ' we obtain, after some algebra, the following expressions for A_L and B_L:

$$\begin{aligned}
A_L e^{-ik_{1z}L} \;=\; & \left(\frac{y_+y_-}{2\gamma_1\nu}\right)\left[I_{\nu-1}(y_-)K_{\nu+1}(y_+) - I_{\nu+1}(y_+)K_{\nu-1}(y_-)\right] \\
& + \left(\frac{\delta_1 y_+}{2\gamma_1}\right)\left[I_{\nu}(y_-)K_{\nu+1}(y_+) + I_{\nu+1}(y_+)K_{\nu}(y_-)\right] \\
& + \left(\frac{\delta_3 y_-}{2\gamma_1}\right)\left[I_{\nu-1}(y_-)K_{\nu}(y_+) + I_{\nu}(y_+)K_{\nu-1}(y_-)\right] \\
& + \left(\frac{\delta_1\delta_3\nu}{2\gamma_1}\right)\left[I_{\nu}(y_-)K_{\nu}(y_+) - I_{\nu}(y_+)K_{\nu}(y_-)\right] \\
B_L e^{ik_{1z}L} \;=\; & -\left(\frac{y_+y_-}{2\gamma_1\nu}\right)\left[I_{\nu+1}(y_-)K_{\nu+1}(y_+) - I_{\nu+1}(y_+)K_{\nu+1}(y_-)\right] \\
& + \left(\frac{\delta_1 y_+}{2\gamma_1}\right)\left[I_{\nu}(y_-)K_{\nu+1}(y_+) + I_{\nu+1}(y_+)K_{\nu}(y_-)\right] \\
& - \left(\frac{\delta_3 y_-}{2\gamma_1}\right)\left[I_{\nu+1}(y_-)K_{\nu}(y_+) + I_{\nu}(y_+)K_{\nu+1}(y_-)\right] \\
& + \left(\frac{\delta_1\delta_3\nu}{2\gamma_1}\right)\left[I_{\nu}(y_-)K_{\nu}(y_+) - I_{\nu}(y_+)K_{\nu}(y_-)\right]
\end{aligned} \tag{20}$$

where $\delta_r = \gamma_r - 1$. Each expression now has potentially three additional terms due to the fact that in the general case $\delta_r \neq 0$.

B. Right Incidence

The set-up for right incidence is shown in Fig. 4.

The algebra follows on similar lines and results in the following expression for A_R, B_R:

$$A_R e^{-ik_{3z}L} \;=\; \left(\frac{y_+y_-}{2\gamma_3\nu}\right)\left[I_{\nu-1}(y_-)K_{\nu+1}(y_+) - I_{\nu+1}(y_+)K_{\nu-1}(y_-)\right]$$

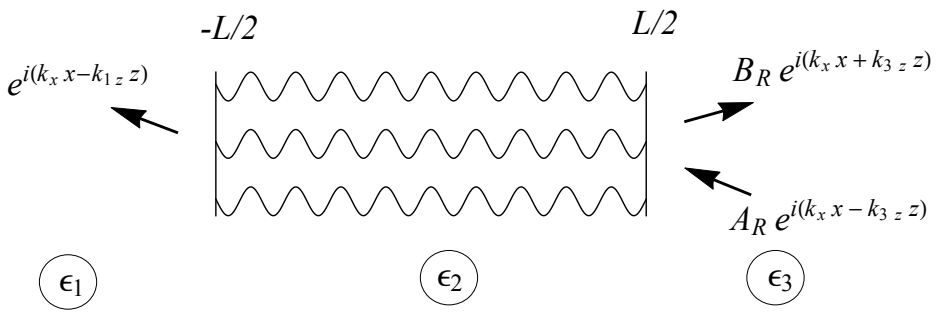

FIG. 4: Generalized set-up for propagation from the right

$$
\begin{aligned}
&+\left(\frac{\delta_3 y_-}{2\gamma_3}\right)[I_\nu(y_+)K_{\nu-1}(y_-)+I_{\nu-1}(y_-)K_\nu(y_+)]\\
&-\left(\frac{\delta_1 y_+}{2\gamma_3}\right)[I_{\nu-1}(y_+)K_\nu(y_-)+I_\nu(y_-)K_{\nu-1}(y_+)]\\
&+\left(\frac{\delta_1\delta_3\nu}{2\gamma_3}\right)[I_\nu(y_-)K_\nu(y_+)-I_\nu(y_+)K_\nu(y_-)]
\end{aligned}
\tag{21}
$$

$$
\begin{aligned}
B_R e^{ik_{3z}L} \;=\;& \left(\frac{y_+ y_-}{2\gamma_3\nu}\right)[I_{\nu-1}(y_+)K_{\nu-1}(y_-)-I_{\nu-1}(y_-)K_{\nu-1}(y_+)]\\
&+\left(\frac{\delta_3 y_-}{2\gamma_3}\right)[I_{\nu-1}(y_-)K_\nu(y_+)+I_\nu(y_+)K_{\nu-1}(y_-)]\\
&-\left(\frac{\delta_1 y_+}{2\gamma_3}\right)[I_\nu(y_-)K_{\nu-1}(y_+)+I_{\nu-1}(y_+)K_\nu(y_-)]\\
&+\left(\frac{\delta_1\delta_3\nu}{2\gamma_3}\right)[I_\nu(y_-)K_\nu(y_+)-I_\nu(y_+)K_\nu(y_-)]
\end{aligned}
$$

Note that, with different background permittivities ε_1 and ε_3, the relation between A_R and A_L is now $|A_L| = (\gamma_3/\gamma_1)|A_R| = (k_{3z}/k_{1z})|A_R|$. This relation can again be obtained by considering the Wronskian of $\psi_L(z)$ and $\psi_R(z)$.

IV. NUMERICAL RESULTS

In this section we explore a variety of different configurations. It should be stressed again that these are configurations which have previously been considered within the Bragg approximation scheme in Ref. [28]. The results can be directly compared[1], and are broadly similar but differ in some details. This is to expected, given the relatively small strength (α^2) of the grating. For larger grating strengths only the present method can be expected to give reliable results, unless several more orders in the Bragg series can be included.

[1] However, the reader should be aware that the convention for a plane wave used in that paper, e^{-jkz}, is opposite to the one used here, namely e^{ikz}, so that left and right are effectively interchanged.

A. Filled-space grating

As the first application of the equations we have derived, we consider oblique incidence on the grating, but keeping the background relative permittivities the same, as in Ref. [26]. In Fig. 5 (left panel) we show the transmission coefficient, which, as already remarked, is the same for left or right incidence. The same characteristic shape that was seen in Ref. [26] is seen again here, but this time as a function of θ rather than k. The transition occurs near $\theta_B = \arccos(\beta/(k\sqrt{\varepsilon_2})) = \arccos(\lambda/(2\Lambda\sqrt{\varepsilon_2})) \approx 1.06$, the angle for which $\nu = 1$. Recall that $\Lambda = \pi/\beta$, the periodicity of the grating. In the right panel we show the left reflection coefficient R_L, which is small, although it increases with larger $|\theta|$, and shows no transition near $\theta = \pm\theta_B$. Thus invisibility from the left is preserved to a large extent, with a small reflection coefficient and a transmission coefficient very close to 1.

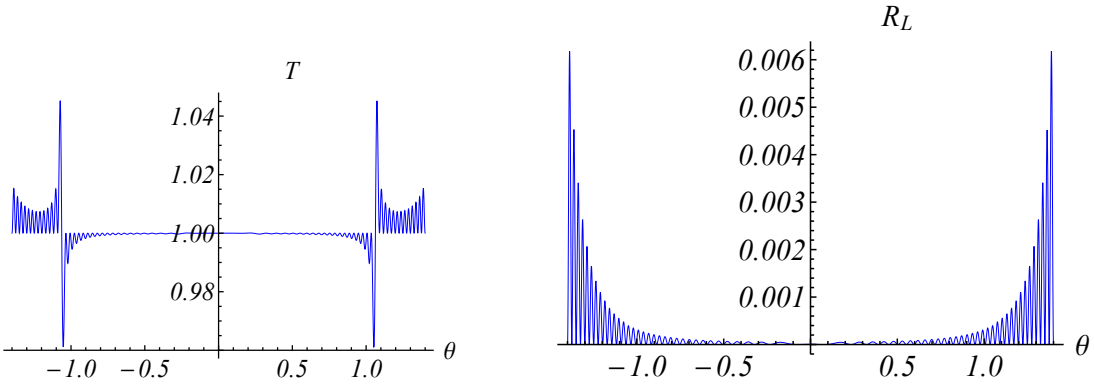

FIG. 5: Transmission coefficient T_L $(= T_R)$ and reflection coefficient R_L as functions of the internal angle of refraction θ for the case $\varepsilon_1 = \varepsilon_2 = \varepsilon_3 = 2.4$. The other parameters are $\alpha^2 = 0.02$, $L = 8.4$, $\Lambda = 0.42$ and $\lambda = 0.633$.

In Fig. 6 we show the right reflection coefficient R_R for the same set of parameters. As a function of θ the right reflection coefficient displays the same high narrow peak that occurs for normal incidence when k is varied. It should be mentioned that these reflection and transmission coefficients satisfy the modified unitarity relation $T - 1 = \pm\sqrt{R_L R_R}$ of Ref. [30] to a high degree of accuracy, which provides a stringent test of our formulas. Note that $T \gtrless 1$ for $|\theta| \gtrless |\theta_B|$.

B. Grating on a slab in air

A rather natural set-up would be for the optical lattice/grating to be implemented on a slab of material with background permittivity ε_2 different from the permittivities on either side. As an example, in this subsection we consider a slab in air, with $\varepsilon_1 = \varepsilon_3 = 1$. It is only to be expected that the reflection and transmission properties will be significantly modified in this case, due to reflections at the interfaces between the different materials. This is indeed borne out by Fig. 7, for the transmission coefficient and the left reflection coefficient.

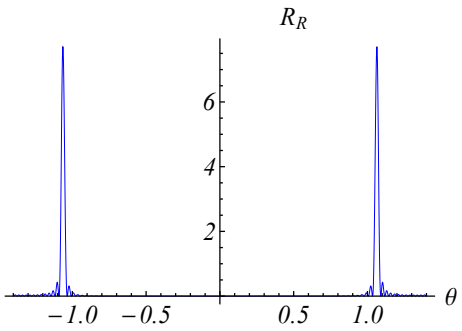

FIG. 6: Right reflection coefficient as a function of the internal angle of refraction θ for the parameters of Fig. 5

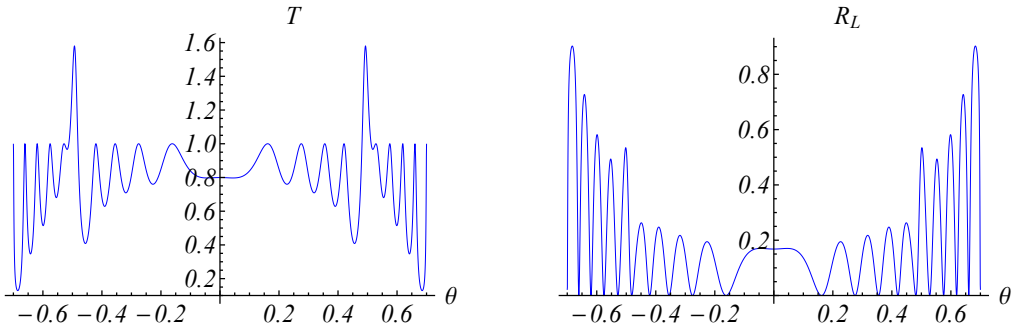

FIG. 7: Transmission coefficient T_L $(= T_R)$ and reflection coefficient R_L as functions of the internal angle of refraction θ for the case $\varepsilon_1 = \varepsilon_3 = 1$, $\varepsilon_2 = 2.4$. The other parameters are $\alpha^2 = 0.02$, $L = 8.28$, $\Lambda = 0.23$ and $\lambda = 0.633$.

However, a more relevant quantity as far as unidirectional invisibility is concerned is the contrast, i.e. the differences $\Delta T \equiv T - T_0$ and $\Delta R_L \equiv R_L - R_0$ where T_0 and R_0 are the transmission coefficients in the absence of the grating, i.e. with $\alpha = 0$. These quantities are shown in Fig. 8, which reveals that ΔT is rather small for $|\theta| \lesssim 0.3$, but becomes appreciable for larger values, and indeed becomes of $O(1)$ in the vicinity of $|\theta| = \theta_B$. The contrast ΔR_L is quite small overall, particularly for $|\theta| \lesssim 0.3$, but shows a significant peak in the vicinity of $|\theta| = \theta_B$.

In Fig. 9 we show the right reflection coefficient, which still shows a characteristic peak near $|\theta| = \theta_B$, but other structure arising from reflection from the boundaries besides.

C. Grating on a substrate

Another natural situation in practice could be for the grating to be implemented on a substrate with a different background permittivity. So, for example, we could have $\varepsilon_1 = 1$,

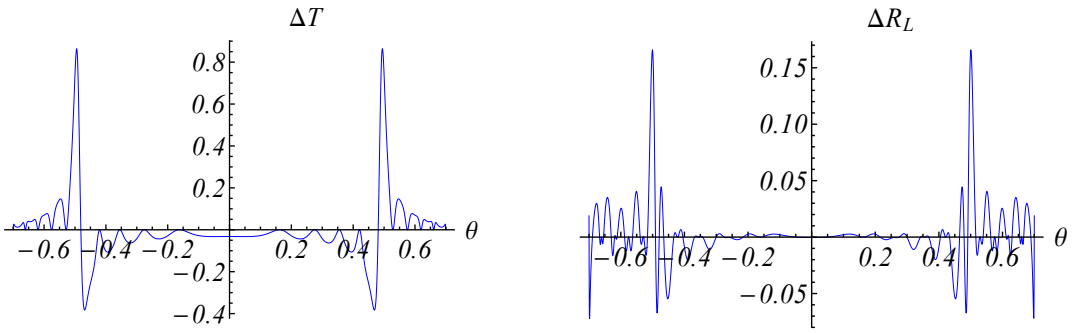

FIG. 8: Contrasts ΔT_L $(= \Delta T_R)$ and ΔR_L as functions of the internal angle of refraction θ for the parameters of Fig. 7.

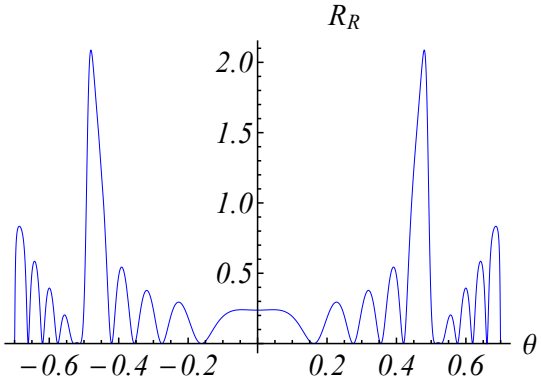

FIG. 9: Right reflection coefficient R_R as a function of the internal angle of refraction θ for the parameters of Fig. 7.

$\varepsilon_2 = 2.4$ and $\varepsilon_3 = 2$, in which case the reflective side of the grating would be attached to the substrate. We could also have the non-reflective side of the grating attached to the substrate, a situation that was considered in Ref. [28], but which we will not discuss here. In this asymmetric case, when $\varepsilon_1 \neq \varepsilon_3$, the set-up is no longer PT symmetric, so that the test of generalized unitarity cannot be applied, and also the relation $T_L = T_R$ no longer holds, as has been previously remarked. One therefore defines the diffraction efficiency for transmission from the left as $\hat{T}_L = (k_{3z}/k_{1z})T_L$ and similarly $\hat{T}_R = (k_{1z}/k_{3z})T_L$, so that $\hat{T}_L = \hat{T}_R$.

Again the reflection and transmission properties are modified, although rather less than in Case B. In Fig. 10 we show the diffaction efficiency for transmission and the left reflection coefficient.

The corresponding contrasts $\Delta\hat{T} \equiv \hat{T} - \hat{T}_0$ and $\Delta R_L \equiv R_L - R_0$ are shown in Fig. 11, from which it can be seen that $|\Delta\hat{T}| \lesssim 0.1$, and is considerably smaller in the region $|\theta| \lesssim 0.3$. The contrast ΔR_L is an order of magnitude smaller.

In Fig. 12 we show the right reflection coefficient, which now has a fairly clean peak near $|\theta| = \theta_B$, with some additional structure for larger $|\theta|$.

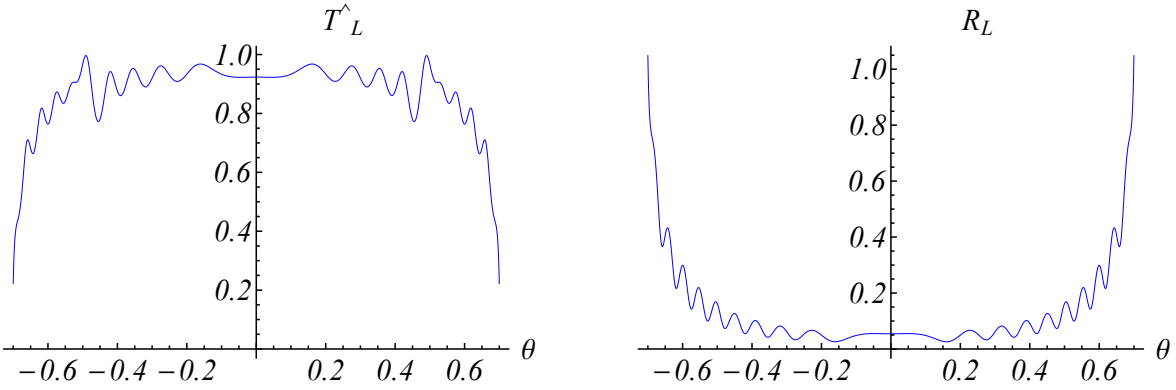

FIG. 10: Diffraction efficiency for transmission $\hat{T}_L$ $(= \hat{T}_R)$ and reflection coefficient R_L as functions of the internal angle of refraction θ for the case $\varepsilon_1 = 1$, $\varepsilon_2 = 2.4$, $\varepsilon_3 = 2$,. The other parameters are as in Fig. 7.

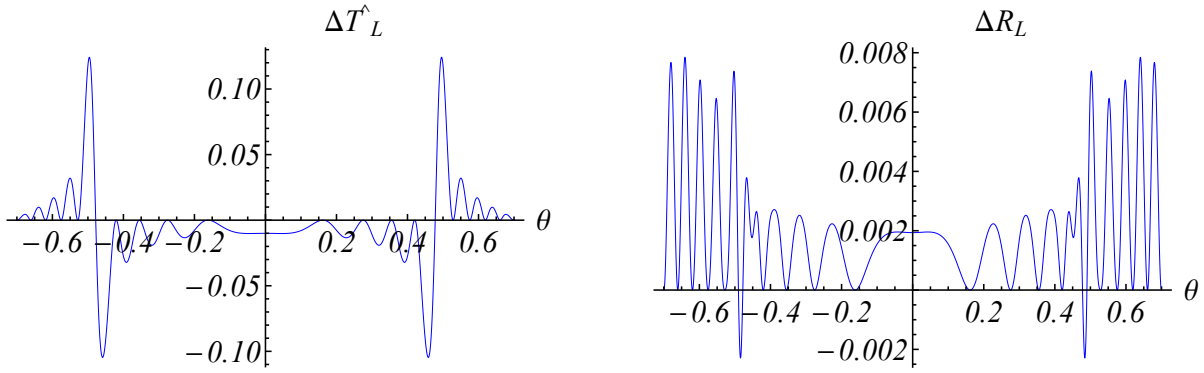

FIG. 11: Contrasts $\Delta\hat{T}_L$ $(= \Delta\hat{T}_R)$ and ΔR_L as functions of the internal angle of refraction θ for the parameters of Fig. 10.

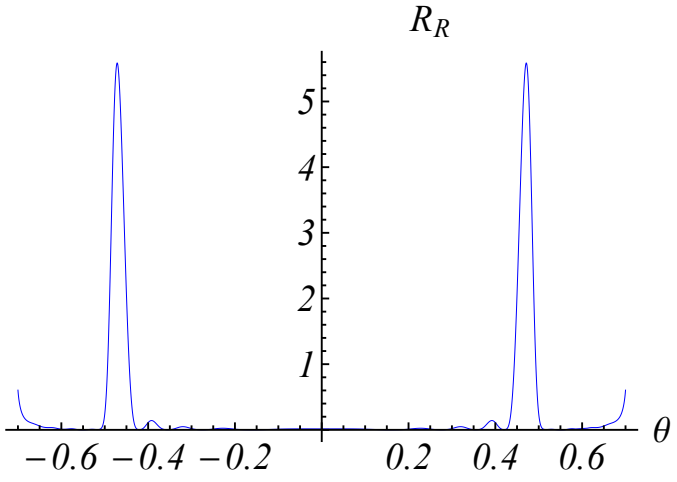

FIG. 12: Right reflection coefficient R_R as a function of the internal angle of refraction θ for the parameters of Fig. 10.

V. MIRROR SET-UP

In this case we revert to normal incidence from the left and take $\varepsilon_3 \to \infty$, corresponding to a perfect dielectric mirror. Then both A_L and B_L tend to infinity because of the terms containing the factor δ_3. We can take out this factor and define $\hat{A}_L = A_L/\delta_3$ and $\hat{B}_L = B_L/\delta_3$, which in this limit are given by

$$\begin{aligned}\hat{A}_L e^{ikL} &= \left(\frac{y_-}{2\gamma_1}\right)[I_{\nu-1}(y_-)K_\nu(y_+) + I_\nu(y_+)K_{\nu-1}(y_-)] \\ &\quad + \left(\frac{\delta_1\nu}{2\gamma_1}\right)[I_\nu(y_-)K_\nu(y_+) - I_\nu(y_+)K_\nu(y_-)] \end{aligned} \tag{22}$$

and

$$\begin{aligned}\hat{B}_L e^{ikL} &= -\left(\frac{y_-}{2\gamma_1}\right)[I_{\nu+1}(y_-)K_\nu(y_+) + I_\nu(y_+)K_{\nu+1}(y_-)] \\ &\quad + \left(\frac{\delta_1\nu}{2\gamma_1}\right)[I_\nu(y_-)K_\nu(y_+) - I_\nu(y_+)K_\nu(y_-)] \end{aligned} \tag{23}$$

Because of the enhanced reflectivity of the grating for right incidence narrowly peaked around $k_2 = \beta$, it seems likely that we will have a resonant cavity near the corresponding frequency, which might well support lasing. For lasing we are looking for a reflection coefficient $|B_L/A_L| = |\hat{B}_L/\hat{A}_L|$ going to infinity, so we are looking for a zero of $\hat{A}_L$, or equivalently of A_R. In Fig. 13 we show R_L as a function of k $(= 2\pi/\lambda)$ for the value of α we have been using throughout the paper. As we can see, this exhibits an extremely sharp peak at a certain value of k, indicating that for that value of k we are very near a zero of $\hat{A}_L$. By fine-tuning α we can find a zero of $\hat{A}_L$ for real k. In fact, the complex zero in k migrates from the lower half-plane to the upper half-plane as α increases, crossing the real axis at the critical value, the lasing threshold. In terms of the transfer matrix, the lasing threshold corresponds as usual to a zero of the element M_{22}.

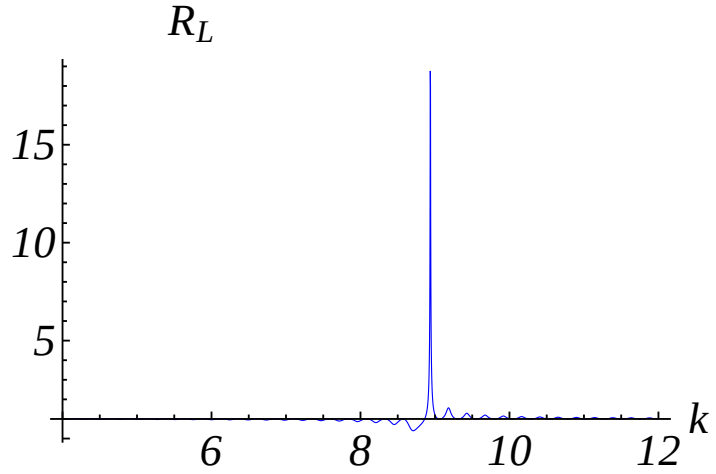

FIG. 13: Left reflection coefficient R_L for normal incidence as a function of k for $\varepsilon_1 = 1$, $\varepsilon_2 = 2.4$ and $\varepsilon_3 \to \infty$. The other parameters are $\alpha^2 = 0.02$, $L = 8.28$ and $\Lambda = 0.23$.

We have analyzed this lasing set-up in more detail in [31] using an extended version of the coupled-wave approximation, and checked the results using the exact formulae presented here. Using the same techniques that were used in Section II we can show that the expression for $\hat{A}_L e^{ikL}$ can be approximated as

$$\hat{A}_L e^{ikL} \sim \frac{1}{4\gamma_1}\left[(1-\gamma_1)e^{ik_2 L} + (1+\gamma_1)\left(e^{-ik_2 L} + \frac{1}{2}ik_2\alpha^2\frac{\sin(L\delta)}{\delta}\right)\right]. \tag{24}$$

If α is real, as has been assumed up to now, the lasing condition on k_2, given by equating the real part of Eq. (24) to zero, is $\cos k_2 L = 0$, which turns out be to exact, but gives multiple competing modes. In order to achieve single-mode lasing we need to shift the overall phase of the grating by $\pi/2$, making α^2 effectively pure imaginary. In that case the lasing condition on k_2, still exact, is given by the imaginary part of the equation, i.e. $\sin k_2 L = 0$, but the real part can only vanish for $\delta = 0$ because of the the zeros of the sinc function. Thus in this configuration the cavity supports single-mode, highly directional, lasing. Both of these properties arise from the particular form of the right reflection coefficient, which to a very good approximation is a sinc function, and is the other side of the coin of the unidirectional invisibility property of the PT-symmetric index profile at the symmetry-breaking point.

The proposed set-up is complementary to other ways of achieving single-mode lasing, exploiting differential PT-symmetry breaking in either a single microring laser[32], or two coupled microring lasers[33]. These set-ups are not unidirectional, however. Yet another way of achieving single-mode unidirectional lasing, in a PT-symmetric chain of disk resonators[34], is to engineer a coincidence of singularities, so that $M_{12} \to \infty$ rather than the usual $M_{22} = 0$.

VI. CONCLUSIONS

We have shown how the exact analytic solutions previously obtained for the one-dimensional grating with index profile proportional to $e^{i\beta z}$ can be generalized to the case of different refractive indices on either side of the grating as well as to non-normal incidence. The resulting formulas for the reflection and transmission amplitudes, Eqs. (20) and (21), contain three additional terms, of the same general form as in the restricted case, but with different indices on the modified Bessel functions I and K. These formulas were used to explore the transmission and reflection characteristics of the grating as a function of incident angle in a variety of situations previously considered within the Bragg approximation scheme, with particular emphasis on the extent to which unidirectional invisibility survives.

The narrow-beam enhanced reflection of the grating for right incidence leads one to suppose that when a mirror is placed to the right of the cavity, the arrangement might support lasing, which calculation using our generalized formulas shows to be indeed the case. More details are given in Ref. [31].

[1] C. M. Bender and S. Boettcher, Phys. Rev. Lett. **80**, 5243 (1998).
[2] C. M. Bender, Contemp. Phys. **46**, 277 (2005); Rep. Prog. Phys. **70**, 947 (2007).
[3] A. Mostafazadeh, Int. J. Geom. Meth. Mod. Phys. **7**, 1191 (2010).
[4] C. M. Bender, D. C. Brody and H. F. Jones, Phys. Rev. Lett. **89**, 270401 (2002) ; 92, 119902(E) (2004).

[5] C. M. Bender, D. C. Brody and H. F. Jones, Phys. Rev. D **70**, 025001 (2004) ; 71, 049901(E) (2005).

[6] A. Mostafazadeh, J. Math. Phys. **43**, 205 (2002); J. Phys. A **36**, 7081 (2003).

[7] A. Ruschhaupt, F. Delgado and J. M. Muga, J. Phys. A **38**, L171 (2005).

[8] R. El-Ganainy, K. G. Makris, D. N. Christodoulides and Z. H. Musslimani, Optics Letters **32**, 2632 (2007).

[9] Z. Musslimani, K. G. Makris, R. El-Ganainy and D. N. Christodoulides, Phys. Rev. Lett. **100**, 030402 (2008).

[10] K. Makris, R. El-Ganainy, D. N. Christodoulides and Z. Musslimani, Phys. Rev. Lett. **100**, 103904 (2008).

[11] S. Klaiman, U. Günther and N. Moiseyev, Phys. Rev. Lett. **101**, 080402 (2008).

[12] A. Guo, G. J. Salamo, D. Duchesne, R. Morandotti, M. Volatier-Ravat, V. Aimez, G. A. Siviloglou and D. N. Christodoulides, Phys. Rev. Lett. **103**, 093902 (2009).

[13] S. Longhi, Phys. Rev. A **81**, 022102 (2010).

[14] K. Makris, R. El-Ganainy, D. N. Christodoulides and Z. Musslimani, Phys. Rev. A **81**, 063807 (2010).

[15] C. Rüter, K G. Makris, R. El-Ganainy, D. N. Christodoulides, M. Segev and D. Kip, Nature Physics **6**, 192 (2010).

[16] H. Ramezani, T. Kottos, R. El-Ganainy and D. N. Christodoulides, Phys. Rev. A **82**, 043803 (2010).

[17] L. Poladian, Phys. Rev. E **54**, 2963 (1996).

[18] M. V. Berry, J. Phys. A **31**, 3493 (1998).

[19] Z. Lin, H. Ramezani, T. Eichelkraut, T. Kottos, H. Cao and D. N. Christodoulides, Phys. Rev. Lett. **106**, 213901 (2011).

[20] N. Midya, B. Roy and R. Roychoudhury, Phys. Lett. A **374**, 2605 (2010).

[21] H. F. Jones, J. Phys. A **45**, 444004 (2012).

[22] M-A. Miri, A. B. Aceves, T. Kottos, V. Kovanis and D. N. Christodoulides, Phys. Rev. A **86**, 033801 (2012).

[23] M. Kulishov, J. Laniel, N. Bélanger, J. Azaña and D. Plant, Opt. Express **13**, 3068 (2005).

[24] L. Feng, Y-L. Xu, W. S. Fwegadolli, M-H. Lu, J. E. B. Oliveira, V. R. Almeida, Y-F. Chen and A. Scherer, Nature Materials **12**, 108 (2013).

[25] S. Longhi, J. Phys. A: Math. Theor. **44**, 485302 (2011).

[26] H. F. Jones, J. Phys. A: Math. Theor. **45**, 135306 (2012).

[27] A. Mostafazadeh, Phys. Rev. A, **89**, 012709 (2014).

[28] M. Kulishov, H. F. Jones and B. Kress, Opt. Express **23**, 18694 (2015).

[29] M. Abramowitz and I. A. Stegun, *Handbook of Mathematical Tables*, Dover, New York 1970.

[30] L. Ge, Y. Chong and A. D. Stone, Phys. Rev. A **85**, 023802 (2012).

[31] H. F. Jones and M. Kulishov, arXiv:1510.08260.

[32] L. Feng, Z. J. Wong, R-M. Ma, Y. Wang, and X. Zhang, Science **346**, 972 (2014).

[33] H. Hodaei, M-A. Miri, M. Heinrich, D. N. Christodoulides and M. Khajavikhan, Science **346**,975 (2014).

[34] H. Ramezani, H-K. Li, Y. Wang and X. Zhang, Phys. Rev. Lett. **113**, 263905 (2014).